applied sciences

MDPI

Article

Characterization of Electromagnetic Pulses Generated from Plasma Associated with Laser Filaments-Excited Aluminum Alloy Interaction

Rong Qi [1,2], Chuliang Zhou [2,*], Dongdong Zhang [2], Liwei Song [2], Xiaojun Yang [2], Jiayan Gui [2], Yuxin Leng [2], Ye Tian [2,*] and Ruxin Li [2,3]

1 School of Physics Science and Engineering, Tongji University, Shanghai 200092, China; qrong0353@sina.com
2 State Key Laboratory of High Field Laser Physics and CAS Center for Excellence in Ultra-Intense Laser Science, Shanghai Institute of Optics and Fine Mechanics (SIOM), Chinese Academy of Sciences (CAS), Shanghai 201800, China; ddzhang@siom.ac.cn (D.Z.); slw@siom.ac.cn (L.S.); yangxiaojun@siom.ac.cn (X.Y.); jygui@siom.ac.cn (J.G.); lengyuxin@mail.siom.ac.cn (Y.L.); ruxinli@mail.siom.ac.cn (R.L.)
3 School of Physical Science and Technology, ShanghaiTech University, Shanghai 200003, China
* Correspondence: chuliangzhou@siom.ac.cn (C.Z.); tianye@siom.ac.cn (Y.T.)

Abstract: Femtosecond laser filament-generated plasma can generate electromagnetic pulses (EMPs). These pulses may reduce the instrument's precision, and, hence, influence the accuracy of the experimental results. They may even cause widespread disruption by disabling of the electronic control systems or distribution networks of power plants. This study investigated the characteristics of EMPs generated from the interaction of filament-generated plasmas with a solid target in air. In this study, ultrafast laser filamentation was used to produce plasma, which was focused on a 3 mm-thick aluminum (Al) alloy target for interaction, and the spatial distribution and main contributors of the EMPs were systematically and extensively studied. The results showed that the EMPs generated from ultrafast laser filament interaction with the Al alloy target had the following characteristics: the EMP energy generated from laser filament interaction with solid targets is tens of times higher than that generated only from the femtosecond laser filament; the maximum EMP signals appeared at a 20°–80° detection angle. The relationship between the energy of EMPs and the width and energy of the laser pulses is presented and discussed. These findings are beneficial for gaining insight into the EMP generation mechanism, spatial distribution, and transmission, and for providing more information for the design of EMPs' shielding.

Keywords: femtosecond laser; filament-generated plasma; solid targets; electromagnetic pulses; laser-plasma interaction

check for updates

Citation: Qi, R.; Zhou, C.; Zhang, D.; Song, L.; Yang, X.; Gui, J.; Leng, Y.; Tian, Y.; Li, R. Characterization of Electromagnetic Pulses Generated from Plasma Associated with Laser Filaments-Excited Aluminum Alloy Interaction. *Appl. Sci.* **2022**, *12*, 6059. https://doi.org/10.3390/app12126059

Academic Editor: Cristian FOCSA

Received: 6 May 2022
Accepted: 13 June 2022
Published: 15 June 2022

1. Introduction

Ultrashort and ultra-intense laser irradiation on solid targets leads to emission of energetic particles, which are also accompanied by broadband electromagnetic pulse radiation [1–6]. The mechanisms that drive these EMPs can differ depending on the interaction conditions, and the EMPs can be emitted at different intensities and frequencies. If strong enough, the EMPs might damage electronics outside and inside the vacuum target chamber and even interfere with power and signal lines, which may further cause perturbation and/or disruption of supply lines and signal communications [7,8]. In these cases, EMPs are generated during the interaction of a powerful laser with a target. The main concern regarding EMPs is their emission when hot electrons cool down over several picoseconds, corresponding to which the frequency range of EMPs decreases from THz to GHz; the EMPs in the GHz range are usually considered the most destructive for electronic circuits [1]. With the invention of chirped pulse amplification (CPA) in lasers [9], the intensity of sub-picosecond (sub-ps) laser systems has progressed significantly. The EMPs in the GHz range

generated by sub-ps laser-solid target interactions are stronger than those generated by nanosecond (ns) laser-solid target interaction. Moreover, it was verified that the GHz EMP source is generated due to the current from the bolster structure to the target. Furthermore, charge separation and target polarization under powerful laser pulse radiation cause the target to be charged by rapid charge accumulation [10]. Therefore, EMPs can be mitigated by controlling the geometrical and electrical characteristics of the target [11,12]. To gain a better understanding of the characteristics and mitigation methods of EMP, substantial efforts have been made in large laser facilities. To date, experimental observations of radio-frequency and microwave radiation from laser-plasma interactions are usually associated with nanosecond to femtosecond pulses directly irradiating solid targets [2,5,13–15].

EMPs usually arise from two mechanisms associated with terawatt- to petawatt-level laser-matter interactions: ionization, via propagation in air, and plasma generation, which is associated with laser-excited solid materials. With the rapid development of femtosecond lasers, the mechanism and characteristics of low-frequency and relatively low-energy EMP produced by femtosecond laser filaments in air have gained attention from researchers [16–21]. When an ultrashort laser pulse above a critical power of several GW is focused onto a spot of tens of micrometers radius, the intensity of the core reaching 10^{13}–10^{14} W/cm^2 [22] is sufficient to ionize the molecules or atoms of the atmosphere [23], forming a plasma [24]. Then, owing to the Kerr effect, a dynamic balance is built between laser beam self-focus and plasma defocus. Finally, the femtosecond laser in the air forms a long-distance plasma channel, namely a femtosecond laser filament. Currently, femtosecond laser filament technology is widely used in astronomy, meteorology, information, medical treatment, industry, and other fields, including artificial rainfall and snow, laser lightning induction, and air waveguide [25–28]. An extension of laser-filament-driven sources of low-frequency radiation below the THz borderline would help avoid strong atmospheric absorption bands that limit long-distance transmission and remote-sensing applications of THz radiation, and would help integrate cutting-edge tools of ultrafast optics and microwave photonics.

Research on EMPs mitigation has been mainly focused on high-energy area EMPs in vacuum. For low-energy area EMPs, which are generated from femtosecond laser air filament-generated plasmas, the focus is more on the mechanism of EMP generation and other laser filament-generated applications [16–20]. However, to date, no systematic research has been conducted to measure EMPs during the process of hundreds of millijoules, femtosecond laser filaments, and solid targets. Understanding the filament-solid interaction is important for EMPs because their intensity strongly depends on the filament-target coupling. Typically, in the short laser pulse domain, for a given pulse duration, the maximum amplitude of the EMP scales linearly with laser pulse energy [1,29]. However, this trend may not be true for filament-solid interactions, because higher laser energies lead to the formation of multiple filaments. To date, the process of scaling of magnitude from picosecond to femtosecond pulse durations remains unclear. A thorough investigation of EMPs generated from laser filament-solid target interaction and their consequences has yet to be conducted. Hence, it is important to extend the study of the characteristics of EMPs generated by femtosecond laser air filamentation to that of the characteristics of EMPs generated by femtosecond laser filament-solid interaction, which would provide a unique opportunity to pursue systematic measurements for the comprehension of ultrashort laser-generated EMPs and their effects.

To gain more insight into the EMP generation mechanism, this study was performed in the 100 terawatt (TW) laser facility at the Shanghai Institute of Optics and Fine Mechanics, Chinese Academy of Sciences [30]. We investigated the characteristics of the EMPs generated from the plasma associated with the laser filaments-excited aluminum (Al) alloy target in air, and confirmed that at the same laser parameters, they are significantly stronger than the EMPs generated from the laser filamentation propagating in air. Additionally, the spatial distribution of the EMPs generated by the interaction between the laser filament and Al alloy target, and the effects of laser pulse duration and laser energy on the EMPs,

were also investigated. The results of this study confirmed that the interference effect of the EMPs on electronics, resulting from the interaction of femtosecond air filamentation with solid targets, cannot be ignored; moreover, we discuss the main factors that mitigate the possible malfunction of electronics due to EMPs generated from femtosecond laser–air filament interaction with solid targets.

2. Experiment

As mentioned earlier, this study was conducted in the TW laser facility at the Shanghai Institute of Optics and Fine Mechanics, Chinese Academy of Sciences. The Ti: sapphire laser had a center wavelength of 800 nm and an adjustable pulse width of 30–300 fs. A schematic of the experimental setup is shown in Figure 1. After a beam splitter, the main laser was focused by an f = 500 mm convex lens, and the laser-induced filaments in air then interacted with a 3 mm thick aluminum alloy target (10 cm × 10 cm × 3 mm) at the middle of the filaments. The resulting EMPs were captured by a biconical antenna (BicoLOG® 20300, operating frequency 20 MHz–3 GHz) in the far field, and monitored by an oscilloscope (1 GHz bandwidth, Tektronix MDO3104 Mixed Domain Oscilloscope, 5 GS/s). RF signatures were acquired in a time-resolved manner by triggering a high-speed digital oscilloscope with a trigger pulse from the laser. The detection distance in the experiment was defined from the laser filaments-target interaction point to the center of the biconical antenna, and the detection angle of the biconical antenna covered 120°–100°, at which the laser propagation axis was set at θ = 0°, and counterclockwise was considered as the positive direction.

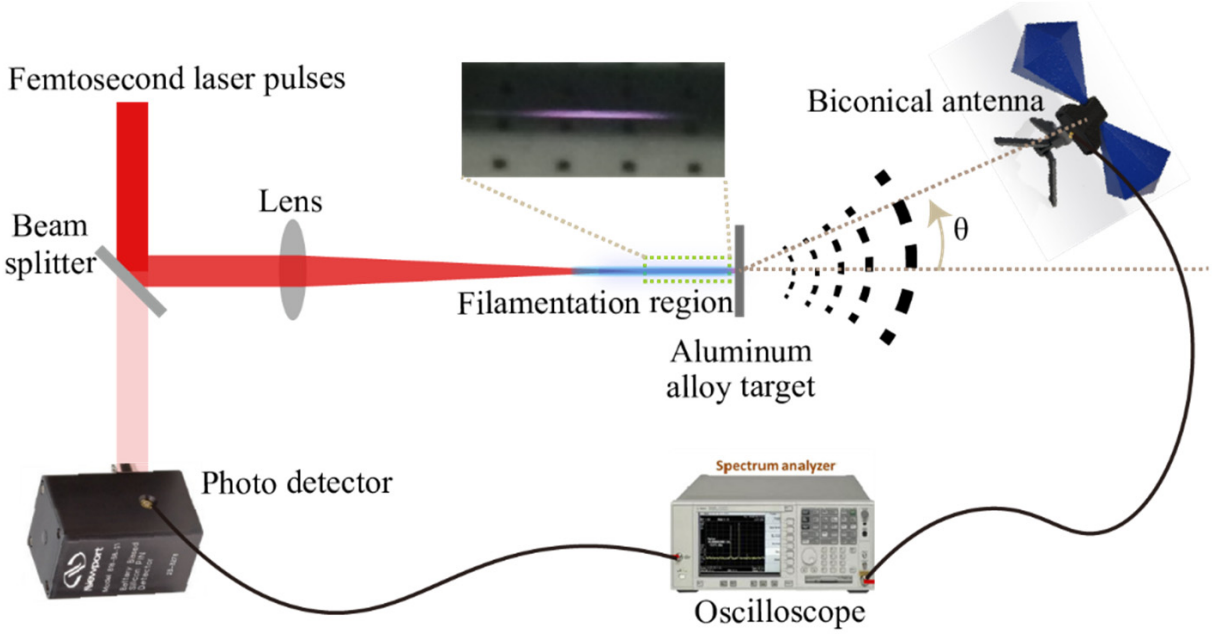

Figure 1. Schematic diagram of the femtosecond laser filament interacting with a solid target.

3. Experimental Results and Discussion

3.1. Distribution of the EMPs in the Time and Frequency Domains

The time-domain signals of EMPs generated from the laser filaments in air and the laser filaments followed by solid targets were measured (as shown in Figure 2a) using the biconical antenna and 1 GHz oscilloscope. Both these measurements were performed under the same following conditions: laser energy E = 850 mJ, laser pulse width t = 30 fs, detection distance d = 50 cm, and detection angle θ = 0°. Figure 2b shows the Fourier transform of the corresponding time-domain signals in Figure 2a. It can be seen that: (1) under the experimental parameters, the amplitude of EMPs generated from the laser filament, followed by a 3 mm-thick alloy target, was approximately 5 times larger than

the peak of the EMPs generated from the laser filament only; (2) the EMPs generated from the laser filament in air were weak and mainly located at 0.19 GHz, whereas those generated from the laser filament–Al alloy target interaction were not only boosted nearby 0.19 GHz, but also had several distinct frequency ranges centered at 0.31 GHz and 0.45 GHz; (3) the amplitude of EMPs from laser filamentation–Al target interaction was approximately 6 times stronger than that of EMPs from laser filamentation in the air. The results showed that the EMPs generated from the laser filaments interacting with the aluminum alloy target were significantly stronger than those generated from the laser filaments only; hence, it is necessary to focus on the EMP generation mechanism from the interactions between femtosecond laser filament and solid targets. It should be noted that this experiment was limited by the oscilloscope bandwidth. In future experiments, we will use an oscilloscope with a higher acquisition frequency to detect EMP signals above 1 GHz. In our experiments, the spectral and waveform amplitude measurements were averaged from 10 laser shots at each condition. In addition, we also calculated the statistical fluctuation of the EMP intensity, the statistical fluctuations of spectral amplitude from shot to shot were about 19.4% with laser energy of 850 mJ, detection distance of 50 cm, and frequency at 0.2 GHz.

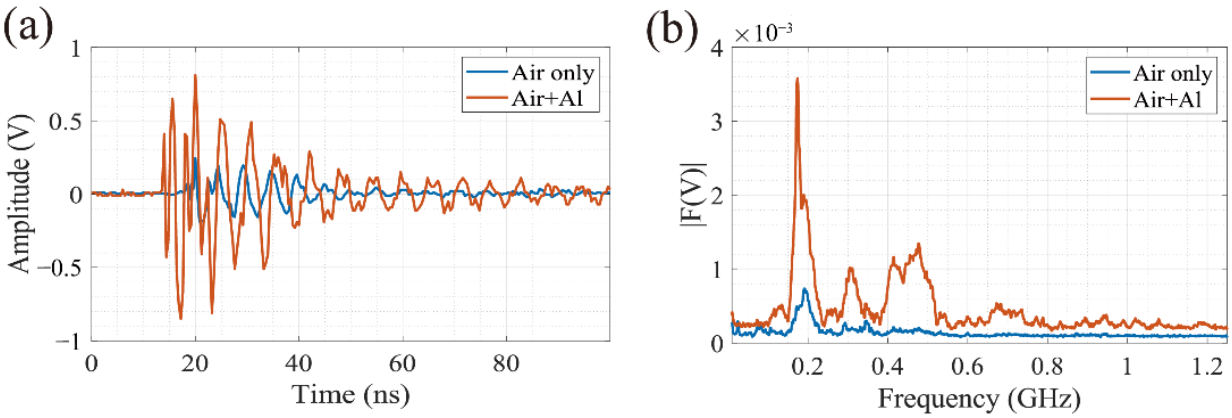

Figure 2. (**a**) Time domain EMP signals measured using the oscilloscope. (**b**) Frequency domain signals, obtained through numerical fast Fourier transform of the time-domain signal. The orange and blue curves correspond to the signals generated from the interaction between laser filament and the 3 mm-thick alloy target and from only the laser filament, respectively. The other experimental parameters were the same: laser energy = 850 mJ, laser pulse width = 30 fs, detection distance = 50 cm, and detection angle = 0°. The spectral and waveform amplitude measurements were averaged from 10 laser shots.

3.2. Spatial Distribution of EMPs

To investigate the spatial distribution characteristics of the EMPs generated from the plasma associated with the laser filament-excited aluminum alloy target in air, we studied the EMP characteristics, which are discussed in the following two sections: the distribution of EMPs with different detection distances and that of EMPs with different detection angles.

3.2.1. Distribution of EMPs with Different Detection Distances

For a laser energy of 170 mJ, laser pulse width of 30 fs and θ = 0°, the EMPs were measured at different distances, ranging from 15 cm to 40 cm, as shown in Figure 3. At different detection distances (15–40 cm), the frequency domain results showed that the main frequency domain of EMP signals appeared at approximately 0.19 GHz. For the EMP at this frequency, the detection distance was relatively small when compared with its wavelength.

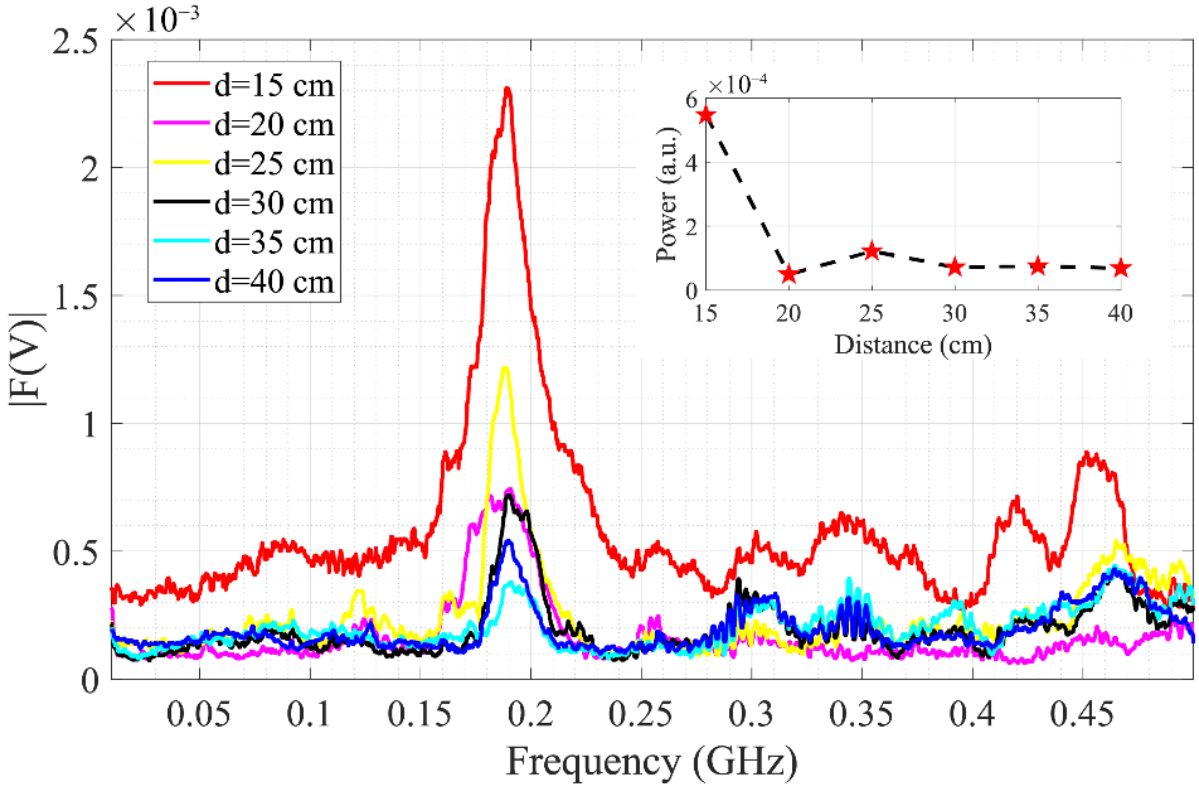

Figure 3. Typical frequency oscillogram of EMP at six values of the distance, where E = 170 mJ, t = 30 fs, d = 15~40 cm, θ = 0° (the inset shows the measured values of the EMP intensity at different detection distance).

The power of EMPs ($\propto \sum V^2 * t$, where the detected voltage V is proportional to the amplitude of the microwave electric field, and, therefore, the microwave power is proportional to the square of V) are shown in the inset of Figure 3; which did not show the expected decreasing trend with increasing detection distance. We analyzed the reason for this and concluded that the detection distance of the antenna in the experiment did not meet the far-field conditions [31].

3.2.2. Distribution of EMPs on Different Angles

The angular distributions of the EMPs were measured at different angles ranging from −120° to 110°, as shown in Figure 4a, and ranging from −120° to 0°, as shown in Figure 4b. The other experimental parameters were as follows: in Figure 4a, E = 100 mJ, t = 30 fs, and d = 20 cm; in contrast, in Figure 4b, the E = 300 mJ, t = 30 fs, and d = 30 cm. Figure 4a shows that the main portion of the power of the EMPs occurred near θ = 70°, which is approximately more than twice as high as at θ = 0° and nearly twice as high as at θ = 90°. In contrast, in Figure 4b, the E was increased from 100 mJ to 300 mJ, and the angular distribution of EMP power ranging from −120° to 0° was measured. As a result, we observed the following: the EMP power increased significantly, from 6×10^{-5} (a.u.) to 3×10^{-3} (a.u.), the EMP energy was more widely distributed with respect to the detection angle, covering −80° to −20°, the strongest signal appeared at θ = −30°, which was approximately twice as high as that at θ = 0° and −90°. In addition, we also measured a strong EMP signal in the backward of the target (near −120°). The corresponding frequency domain signals are shown in Figure 4c. Moreover, the main frequency domain was at 0.19 GHz, and there was also a significant EMP signal near 0.45 GHz.

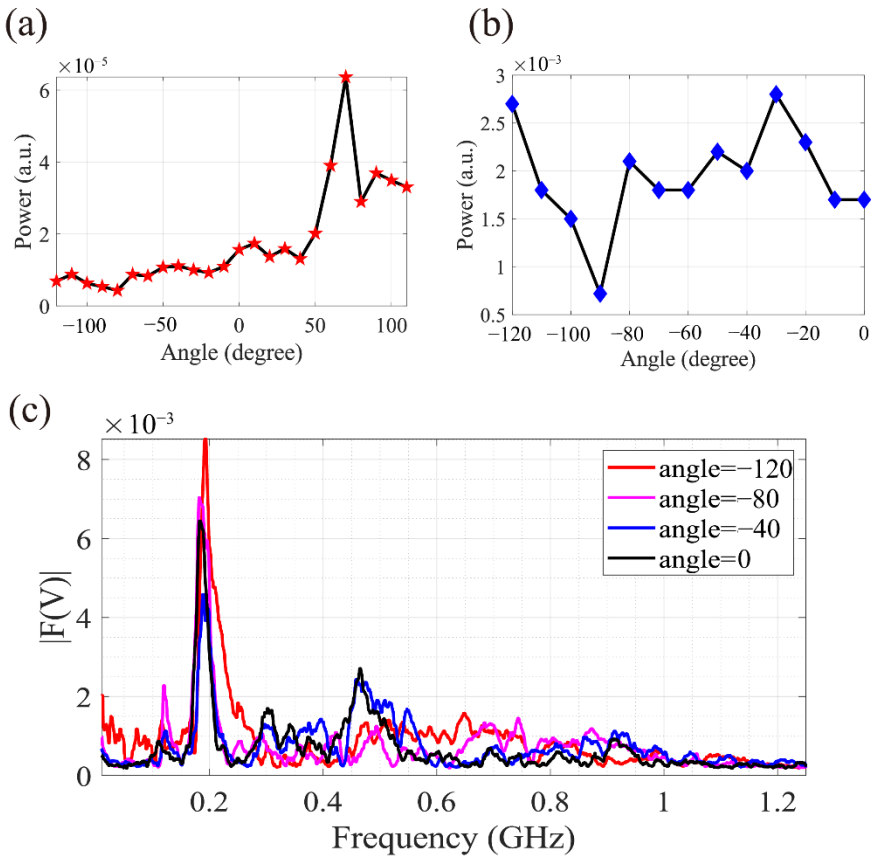

Figure 4. (**a**) Measured angular distributions of EMPs in the detection plane (E = 100 mJ, t = 30 fs, d = 20 cm, and θ ranging from −120° to 110°). (**b**) Measured angular distributions of EMPs in the detection plane (E = 300 mJ, t = 30 fs, d = 30 cm, and θ ranging from −120° to 0°). (**c**) Frequency-domain signals for different angles (E = 300 mJ, the t = 30 fs, and d = 30 cm).

3.3. Effect of Different Laser Pulse Widths on EMPs

As explained in Section 3.1, femtosecond laser filament interaction with solid targets produced intense EMPs. Furthermore, we examined the effect of different laser pulse widths on the generation of EMPs, while keeping other experimental conditions unchanged (E = 485 mJ, θ = 0°, and d = 65 cm). We adjusted the laser pulse width to 30, 156, 195, 231, and 300 fs, respectively, and the experimental results showed that the power of the EMPs weakly decreased with increasing laser pulse width, following an approximately linear trend, as shown in Figure 5a. This can be interpreted as follows: the main EMP generation mechanism is believed to be the laser-induced ponderomotive force electromagnetic potential driving the free electrons away from the laser focus in the radial and axial directions [18], and the intensity of the EMPs is mainly determined by the balance between the production rate of the induced stripped free electrons and the annihilation rate of such free electrons. At the same energy, a shorter laser pulse will lead to a higher production rate of free electrons, while the annihilation rate of such electrons in the same experimental setup and experimental space remains constant; as a result, the EMPs will decrease as the laser pulse width is increased at the same energy. In this experiment, the frequencies of EMPs generated at different laser pulse widths were mainly concentrated at approximately 0.19 GHz, and there were also significant EMPs generated at approximately 0.28 GHz, in the 0.3–0.4 GHz frequency band, and at approximately 0.48 GHz (Figure 5b); and the EMP spectrum did not change significantly with the femtosecond laser pulse width. The main reason for the latter is that the main factors affecting the EMPs produced by the interaction between femtosecond laser filament and the target are hot electron emission and electron reflux.

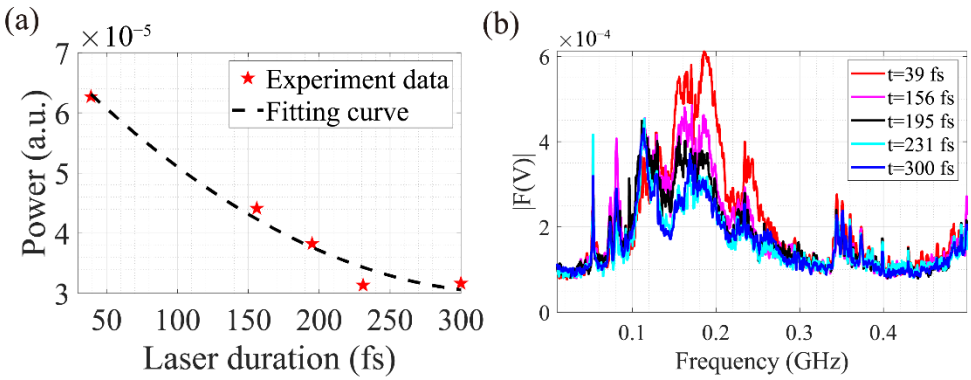

Figure 5. (**a**) The total power of EMPs as a function of t. (**b**) Fourier spectra of the EMP signals for various values of t. The corresponding experimental parameters are: E = 485 mJ, θ = 0°, d = 65 cm, and the different values of t are 39, 156, 195, 231, 300 fs.

3.4. Dependence of the Power of EMPs on the Laser Pulse Energy

In this study, the effect of the EMPs amplitudes versus different laser energies of 240, 300, 600, and 850 mJ were measured while keeping the other experimental parameters constant: t = 30 fs, θ = 0°, and d = 40 cm (Figure 6). From 240 mJ to 850 mJ, the amplitude of EMPs increased with the laser pulse energy at a given pulse width (Figure 6a). In other words, a significant increase in the amplitude of EMPs occurred in the laser energy interval of 240–600 mJ, while the growth trend of this amplitude slowed down in the laser energy interval of 600–850 mJ. This was mainly because under the experimental conditions of t = 30 fs, θ = 0°, and d = 30 cm, the EMPs generated by the interaction between femtosecond laser filament 3 mm-thick aluminum target gradually saturated around the laser energy of 600 mJ, and the increase in laser energy was no longer a decisive factor for EMP enhancement. The corresponding spectrum is shown in Figure 6b, which shows that the frequency domain near 0.19 GHz was still the most dominant contribution. In addition, a significant EMP signal also appeared near 0.31 GHz, and a more significant EMP signal appeared near 0.45 GHz for the low laser energy.

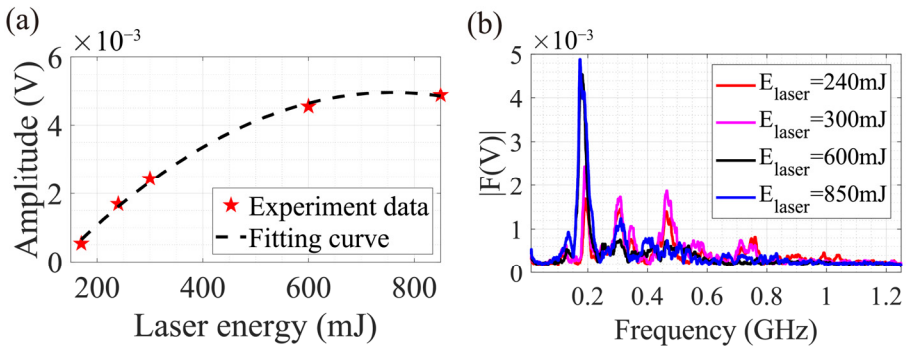

Figure 6. (**a**) The amplitude of EMPs as a function of laser energy. (**b**) Comparison of EMP spectra for four laser energies. The corresponding parameters are: t = 30 fs, d = 40 cm, θ = 0°, and different values of E are 240, 300, 600, 850 mJ.

The power of the EMPs produced by interaction between the femtosecond laser filamentation and a 3 mm-thick aluminum target was tens of times stronger than the EMP produced by the femtosecond laser interacting with air under the same laser parameters, using the EMP laser-guided filamentation energy conversion efficiency mode [18]:

$$\eta_{power} = \frac{P_{EMP}}{P_L} \sim \frac{\pi^2}{8}\left(\frac{a_L\lambda_0}{c\tau_L}\right)^2\left(\frac{2N_p r_p c\tau_L + r_p^2}{R^2}\right)$$

where, a_L is the laser strength parameter, λ_0 is the laser wavelength, and τ_L is laser pulse duration. In our experiment, the laser wavelength was $\lambda_0 = 0.8$ μm, the laser strength parameter was $a_L = \frac{q|E_L|}{mc\omega_0} \sim 5.7 \times 10^{-3}$, the number of plasma wavelengths behind the pulse was $(N_p) \sim 1$, the plasma filament spot size was $(r_p) \sim 100$ μm, the laser focus spot was $(R) \sim 200$ μm, and the laser pulse duration was $\tau_L = 30$ fs. It could be estimated that the EMP energy efficiency of laser filament formation in this experiment could reach $\eta_{EMP\_air} = 7.5 \times 10^{-8}$, and it was thus estimated that the EMP energy efficiency generated by the laser filamentation and the action of the 3 mm-thick aluminum target could reach $\eta_{EMP_{air+Al}} \sim 10^{-6}$. Furthermore, the EMP intensity was proportional to the laser pulse intensity and energy, which was consistent with the results of other studies on short laser pulses [10] and those on high power ps lasers [11].

For interaction between femtosecond laser filament and a metal target, the EMP generated by the plasma channel, owing to the femtosecond laser air filamentation effect, was only a tiny fraction of the overall EMP. A vast majority of the EMP came from the contribution of hot electron excitation and electron reflux generated by the interaction of the femtosecond laser air filamentation with the metal target. The hot electrons radiated part of the energy in the form of bremsstrahlung radiation, covering a wide range of spectra. In our experiments, we observed the following: (1) by using femtosecond laser air filamentation and a 3 mm-thick planar aluminum target, a broad spectrum EMP of 0.1–1.0 GHz could be produced, and the main characteristic spectrum appeared at approximately 0.19 GHz, for the femtosecond laser pulse. This was because the target discharge time had the order of 100 ps; moreover, the effect of the laser pulse width on the frequency domain of the EMP was not obvious; (2) using the EMP frequency calculation formula [1]: fs = $c/(4 \times (ls + ds/2))$ for grounding the conductive plate, where c is the speed of light, the length of the grounding line (ls) = 30 cm, and the length of the square side of the aluminum target (ds) = 10 cm, the experimentally generated EMP frequency could be estimated to be 0.214 GHz, which matched the experimentally obtained EMP frequency, which was mainly concentrated at 0.19 GHz.

4. Conclusions

This study was focused on the characteristics of EMPs generated from the plasma associated with the laser filament-excited aluminum alloy target in air. We measured the time and frequency domain characteristics of the EMP. It was found that its main characteristic frequency was at 0.19 GHz, and a theoretical explanation for this observation was provided. The intensity of EMPs generated from the plasma associated with the ultrashort laser filament-excited aluminum alloy target in air was tens of times higher than that generated from the plasma associated only with ultrashort laser filaments. Besides, the angular distribution and the effect of detection distance were also measured. The measured power of EMPs did not show the expected decreasing trend with increasing detection distance (15–40 cm), and the EMP signals were mainly emitted toward the 70° direction. In addition, the effects of laser pulse duration and laser energy on EMPs were also investigated. As the laser pulse duration increased, the intensity of EMPs was found to decrease following a weak linear trend. Moreover, the intensity of EMPs was observed to be positively correlated with the laser energy, with the rate of increase slowing down at approximately 600 mJ. Obviously, more experiments regarding the influence of laser parameters and the type of target material on the temporal characteristics of EMPs are required to fully understand the EMP emission mechanism, especially for EMPs that are generated from the plasma associated with ultrashort laser filament-excited solid material.

Author Contributions: Conceptualization, Y.T.; Formal analysis, R.Q. and C.Z.; Funding acquisition, C.Z., Y.L. and Y.T.; Investigation, R.Q., C.Z., D.Z., X.Y. and J.G.; Methodology, L.S.; Supervision, Y.L., Y.T. and R.L.; Visualization, R.Q. and C.Z.; Writing—original draft, R.Q.; Writing—review & editing, C.Z. and Y.T. All authors have read and agreed to the published version of the manuscript.

Funding: This work has received funding from the National Natural Science Foundation of China (grants No. 11922412, 11874372), Young Talents Support Project of China Association for Science and Technology, Shanghai Pilot Program for Basic Research—Chinese Academy of Science, Shanghai Branch. Key Research Program of Frontier Sciences, Chinese Academy of Science and Youth Innovation Promotion Association of Chinese Academy of Sciences.

Institutional Review Board Statement: Not applicable.

Informed Consent Statement: Not applicable.

Data Availability Statement: The data that support the findings of this study are available from the corresponding author upon reasonable request.

Acknowledgments: The authors gratefully acknowledge fruitful discussions with Tiejun Wang.

Conflicts of Interest: The authors declare no conflict of interest.

References

1. Consoli, F.; Tikhonchuk, V.T.; Bardon, M.; Bradford, P.; Carroll, D.C.; Cikhardt, J.; Cipriani, M.; Clarke, R.J.; Cowan, T.E.; Danson, C.N.; et al. Laser produced electromagnetic pulses: Generation, detection and mitigation. *High Power Laser Sci. Eng.* **2020**, *8*, e22. [CrossRef]
2. Consoli, F.; De Angelis, R.; Andreoli, P.; Cristofari, G.; Di Giorgioa, G. Measurement of the Radiofrequency-microwave Pulse Produced in Experiments of Laser-plasma Interaction in the ABC Laser Facility. *Phys. Procedia* **2015**, *62*, 11–17. [CrossRef]
3. Prencipe, I.; Fuchs, J.; Pascarelli, S.; Schumacher, D.W.; Stephens, R.B.; Alexander, N.B.; Briggs, R.; Büscher, M.; Cernaianu, M.O.; Choukourov, A.; et al. Targets for high repetition rate laser facilities: Needs, challenges and perspectives. *High Power Laser Sci. Eng.* **2017**, *5*, e17. [CrossRef]
4. Brown, C.G.; Throop, A.; Eder, D.; Kimbrough, J. Electromagnetic pulses at short-pulse laser facilities. *J. Phys. Conf. Ser.* **2008**, *112*, 032025. [CrossRef]
5. Raczka, P.; Cikhardt, J.; Pfeifer, M.; Krasa, J.; Krupka, M.; Burian, T.; Krus, M.; Pisarczyk, T.; Dostal, J.; Dudzak, R.; et al. Measurement of strong electromagnetic pulses generated from solid targets at sub-ns kJ-class PALS laser facility. *Plasma Phys. Control. Fusion* **2021**, *63*, 085015. [CrossRef]
6. Xia, Y.; Zhang, F.; Cai, H.; Zhou, W.; Tian, C.; Zhang, B.; Liu, D.; Yi, T.; Xu, Y.; Wang, F.; et al. Analysis of electromagnetic pulses generation from laser coupling with polymer targets: Effect of metal content in target. *Matter Radiat. Extrem.* **2020**, *5*, 017401. [CrossRef]
7. Bardon, M.; Etchessahar, B.; Lubrano, F.; Bazzoli, S.; Ferri, M.; Ribolzi, J.; Mirabel, P.; La Fontaine, A.C.; Mallejac, N.; Cadra, S.; et al. Mitigation of strong electromagnetic pulses on the LMJ-PETAL facility. *Phys. Rev. Res.* **2020**, *2*, 033502. [CrossRef]
8. Eder, D.C.; Throop, A.; Brown, C.G., Jr.; Kimbrough, J.; Stowell, M.L.; White, D.A.; Song, P.; Back, N.; Macphee, A.; Chen, H.; et al. *Mitigation of Electromagnetic Pulse (EMP) Effects from Short-Pulse Lasers and Fusion Neutrons*; Lawrence Livermore National Lab. (LLNL): Livermore, CA, USA, 2009.
9. Strickland, D.; Mourou, G. Compression of amplified chirped optical pulses. *Opt. Commun.* **1985**, *56*, 219–221. [CrossRef]
10. Dubois, J.-L.; Lubrano-Lavaderci, F.; Raffestin, D.; Ribolzi, J.; Gazave, J.; La Fontaine, A.C.; D'Humières, E.; Hulin, S.; Nicolaï, P.; Poyé, A.; et al. Target charging in short-pulse-laser–plasma experiments. *Phys. Rev. E* **2014**, *89*, 013102. [CrossRef]
11. Bradford, P.; Woolsey, N.C.; Scott, G.G.; Liao, G.; Liu, H.; Zhang, Y.; Zhu, B.; Armstrong, C.; Astbury, S.; Brenner, C.; et al. EMP control and characterization on high-power laser systems. *High Power Laser Sci. Eng.* **2018**, *6*, e21. [CrossRef]
12. Price, C.J.; Donnelly, T.D.; Giltrap, S.; Stuart, N.; Parker, S.; Patankar, S.; Lowe, H.; Drew, D.; Gumbrell, E.T.; Smith, R.A. An in-vacuo optical levitation trap for high-intensity laser interaction experiments with isolated microtargets. *Rev. Sci. Instrum.* **2015**, *86*, 033502. [CrossRef] [PubMed]
13. Robinson, T.S.; Consoli, F.; Giltrap, S.; Eardley, S.J.; Hicks, G.; Ditter, E.J.; Ettlinger, O.; Stuart, N.H.; Notley, M.; De Angelis, R.; et al. Low-noise time-resolved optical sensing of electromagnetic pulses from petawatt laser-matter interactions. *Sci. Rep.* **2017**, *7*, 983. [CrossRef] [PubMed]
14. Seimetz, M.; Bellido, P.; Mur, P.; Lera, R.; La Cruz, A.R.-D.; Sánchez, I.; Zaffino, R.; Benlliure, J.; Ruiz, C.; Roso, L.; et al. Electromagnetic pulse generation in laser-proton acceleration from conductive and dielectric targets. *Plasma Phys. Control. Fusion* **2020**, *62*, 115008. [CrossRef]
15. Rączka, P.; Dubois, J.; Hulin, S.; Rosiński, M.; Ryć, L.; Parys, P.; Zaraś-Szydłowska, A.; Terwińska, D.; Tchórz, P.; Badziak, J.; et al. Target Charging, Strong Electromagnetic Pulse Emission and Proton Acceleration from Thin Foils at 10 TW IPPLM Femtosecond Laser Facility. *Acta Phys. Pol. A* **2020**, *138*, 593–600. [CrossRef]
16. Hosseini, S.; Ferland, B.; Chin, S. Measurement of filament length generated by an intense femtosecond laser pulse using electromagnetic radiation detection. *Appl. Phys. A* **2003**, *76*, 583–586. [CrossRef]
17. Peñano, J.R.; Sprangle, P.; Hafizi, B.; Ting, A.; Gordon, D.F.; Kapetanakos, C.A. Propagation of ultra-short, intense laser pulses in air. *Phys. Plasmas* **2004**, *11*, 2865–2874. [CrossRef]

18. Sprangle, P.; Peñano, J.R.; Hafizi, B.; Kapetanakos, C.A. Ultrashort laser pulses and electromagnetic pulse generation in air and on dielectric surfaces. *Phys. Rev. E* **2004**, *69*, 066415. [CrossRef]
19. Couairon, A.; Franco, M.; Méchain, G.; Olivier, T.; Prade, B.; Mysyrowicz, A. Femtosecond filamentation in air at low pressures: Part I: Theory and numerical simulations. *Opt. Commun.* **2006**, *259*, 265–273. [CrossRef]
20. Lubenko, D.; Alekseev, S.; Sandabkin, E.; Losev, V. Generation of thz emission in femtosecond laser-induced filament. In Proceedings of the XV International Conference on Pulsed Lasers and Laser Applications, (SPIE 2021), Tomsk, Russia, 12–17 September 2021.
21. Englesbe, A.; Elle, J.; Schwartz, R.; Garrett, T.; Woodbury, D.; Jang, D.; Kim, K.-Y.; Milchberg, H.; Reid, R.; Lucero, A.; et al. Ultrabroadband microwave radiation from near- and mid-infrared laser-produced plasmas in air. *Phys. Rev. A* **2021**, *104*, 013107. [CrossRef]
22. Kasparian, J.; Sauerbrey, R.; Chin, S. The critical laser intensity of self-guided light filaments in air. *Appl. Phys. A* **2000**, *71*, 877–879. [CrossRef]
23. Couairon, A.; Mysyrowicz, A. Femtosecond filamentation in transparent media. *Phys. Rep.* **2007**, *441*, 47–189. [CrossRef]
24. Liu, Y.; Chen, Z.; Shi, J. Research progress on electromagnetic wave transmission via femtosecond-laser plasma channel. *Laser Optoelectron. Prog.* **2019**, *56*, 16–26.
25. Polynkin, P. Multi-pulse scheme for laser-guided electrical breakdown of air. *Appl. Phys. Lett.* **2017**, *111*, 161102. [CrossRef]
26. Johnson, L.A.; Sprangle, P.; Hafizi, B.; Ting, A. Remote atmospheric optical magnetometry. *J. Appl. Phys.* **2014**, *116*, 064902. [CrossRef]
27. Liu, Y.; Sun, H.; Liu, J.; Liang, H.; Ju, J.; Wang, T.; Tian, Y.; Wang, C.; Liu, Y.; Chin, S.L.; et al. Laser-filamentation-induced water condensation and snow formation in a cloud chamber filled with different ambient gases. *Opt. Express* **2016**, *24*, 7364–7373. [CrossRef]
28. Ackermann, R.; Stelmaszczyk, K.; Rohwetter, P.; Méjean, G.; Salmon, E.; Yu, J.; Kasparian, J.; Méchain, G.; Bergmann, V.; Schaper, S.; et al. Triggering and guiding of megavolt discharges by laser-induced filaments under rain conditions. *Appl. Phys. Lett.* **2004**, *85*, 5781–5783. [CrossRef]
29. Mondal, S.; Shirozhan, M.; Ahmed, N.; Bocoum, M.; Boehle, F.; Vernier, A.; Haessler, S.; Lopez-Martens, R.; Sylla, F.; Sire, C.; et al. Surface plasma attosource beamlines at ELI-ALPS. *J. Opt. Soc. Am. B* **2018**, *35*, A93–A102. [CrossRef]
30. Wu, F.; Zhang, Z.; Yang, X.; Hu, J.; Ji, P.; Gui, J.; Wang, C.; Chen, J.; Peng, Y.; Liu, X.; et al. Performance improvement of a 200TW/1Hz Ti:sapphire laser for laser wakefield electron accelerator. *Opt. Laser Technol.* **2020**, *131*, 106453. [CrossRef]
31. Stutzman, W.L.; Thiele, G.A. *Antenna Theory and Design*; John Wiley & Sons: New York, NY, USA, 1998.